

Determining our peculiar velocity from the aberration in the cosmic microwave background

R. Aurich and D. Reinhardt

*Institut für Theoretische Physik, Universität Ulm,
Albert-Einstein-Allee 11,
D-89069 Ulm, Germany*

arXiv:2103.08248v2 [astro-ph.CO] 22 Jul 2021

ABSTRACT

The motion of our solar system relative to the cosmic microwave background (CMB) rest frame leads to subtle distortions in the observed CMB sky map due to the aberration effect. Usually the corresponding peculiar velocity is determined from the CMB dipole but neglecting intrinsic dipole contributions. Here it is investigated whether certain invariant scalar measures, which are derived from first and second order covariant derivatives on the sphere, can detect the distortions caused by the aberration effect at high multipoles. This would in principle allow to disentangle the Doppler from intrinsic dipole contributions providing an independent method for the determination of our peculiar velocity. It is found that the eigenvalues of the Hessian matrix of the temperature field are well suited for that task.

Key words: Cosmology, cosmic background radiation

1 INTRODUCTION

On the theoretical side the fluctuations in the cosmic microwave background (CMB) radiation are usually computed in the rest frame of the CMB with computer programs such as CAMB. However, on the observational side, one has to take into account our peculiar velocity with respect to the rest frame of the CMB. This leads to the large Doppler dipole contribution in the CMB on which the usual determination of our velocity is based. For further cosmological CMB analysis this contribution is ignored.

The peculiar velocity is defined as the velocity of our solar system barycentre relative to the CMB rest frame, which in turn is defined by the vanishing of the temperature dipole a_{1m} . These coefficients are extracted from the spherical expansion of the temperature fluctuations

$$\delta T(\vartheta, \varphi) = \sum_{\ell, m} a_{\ell m} Y_{\ell m}(\vartheta, \varphi) \quad , \quad (1)$$

where $Y_{\ell m}(\vartheta, \varphi)$ are the spherical harmonics. The COBE mission determined the peculiar velocity as $\beta_{\odot} = 0.00123$ in the direction $(l, b) \simeq (264^{\circ}, 48^{\circ})$ in galactic coordinates (Kogut et al. 1993), where $\beta := v/c$ is the velocity in units of the speed of light c .

If $T^{(\text{rest})}$ and $\hat{n}^{(\text{rest})}$ denote the CMB rest frame temperature and the unit vector of the considered direction, respectively, then a Lorentz transformation according to the peculiar velocity $\vec{\beta}$ leads to the transformed temperature (Challinor & van Leeuwen 2002)

$$T^{(\text{obs})}(\hat{n}^{(\text{obs})}) = \frac{T^{(\text{rest})}(\hat{n}^{(\text{rest})})}{\gamma(1 - \hat{n}^{(\text{obs})} \cdot \vec{\beta})} \quad (2)$$

in the frame of the observer, who measures $T^{(\text{obs})}(\hat{n}^{(\text{obs})})$

in the direction $\hat{n}^{(\text{obs})}$ and $\gamma := (1 - \beta^2)^{-1/2}$. It is instructive to consider this expression in linear order of β , which leads to the temperature fluctuations (see e.g. Planck Collaboration: Aghanim et al. (2014))

$$\begin{aligned} \delta T^{(\text{obs})}(\hat{n}^{(\text{obs})}) &= T_0 \hat{n}^{(\text{obs})} \cdot \vec{\beta} \\ &+ \delta T^{(\text{rest})}(\hat{n}^{(\text{obs})} - \nabla \hat{n}^{(\text{obs})} \cdot \vec{\beta}) (1 + \hat{n}^{(\text{obs})} \cdot \vec{\beta}) \quad , \quad (3) \end{aligned}$$

where T_0 denotes the CMB mean temperature. The first term on the right hand side of eq. (3) is the usual Doppler dipole which has an amplitude of $T_0 \beta_{\odot} \simeq 3352 \mu\text{K}$. The argument of the temperature fluctuation $\delta T^{(\text{rest})}$ in eq. (3) is aberrated by the deflection $\nabla \hat{n}^{(\text{obs})} \cdot \vec{\beta}$. Furthermore, this amplitude is also modulated by the factor $(1 + \hat{n}^{(\text{obs})} \cdot \vec{\beta})$. The numerical analysis in this work is based on the complete formula (2) and not on the linear approximation. The angular power spectrum $\mathcal{D}_{\ell} = \ell(\ell+1)C_{\ell}/(2\pi)$ with $C_{\ell} = \sum_m |a_{\ell m}|^2/(2\ell+1)$ possesses for small multipole orders $2 < \ell \lesssim 10$ values around $1000 \mu\text{K}^2$ (Planck Collaboration: Akrami et al. 2020). Assuming that the intrinsic dipole \mathcal{D}_1 is of the same order, one is lead to the expectation $C_1 = \pi \mathcal{D}_1 \simeq \pi 1000 \mu\text{K}^2$ and thus to a dipole amplitude $\sqrt{C_1} \simeq 56 \mu\text{K}$. An intrinsic dipole of the primordial temperature anisotropy field is therefore expected to be at the 1% level with respect to the Doppler dipole $T_0 \beta_{\odot}$.

Although intrinsic dipole of the primordial temperature anisotropy field is considered as negligible, the observed CMB power spectrum reveals a parity asymmetry and possesses multipoles C_{ℓ} with enhanced power for odd multipoles ℓ and reduced power for the even ones for not too high values of ℓ corresponding to the largest angular scales (Land & Magueijo 2005; Kim & Naselsky 2010; Planck Collaboration: Akrami et al. 2020). And since the dipole is an odd multipole, of course, it could be larger than the expected 1% level.

Due to the inability to disentangle the Doppler contribution from other dipole contributions, it would thus be favourable to derive the peculiar velocity from an alternative way. This is offered by the fact that the aberration due to the peculiar velocity induces a stretching and a compression of the CMB structures in sky maps, which depends on the angular distance from the direction of our peculiar velocity, in addition to the modulation described above. These modifications of the CMB structures occur for a velocity β of the order 10^{-3} at very high multipoles $\ell \gtrsim 1000$. Based on eq. (2), they are described by the aberration kernel $K_{\ell m}^{\ell' m'}(\beta)$ (Challinor & van Leeuwen 2002) of the multipole transformation law

$$a_{\ell m}^{(\text{obs})} = \sum_{\ell', m'} K_{\ell m}^{\ell' m'}(\beta) a_{\ell' m'}^{(\text{rest})} \quad , \quad (4)$$

where $a_{\ell m}^{(\text{rest})}$ are the multipole expansion coefficients in the CMB rest frame and $a_{\ell m}^{(\text{obs})}$ are those observed in the moving frame. The double sum in eq. (4) reduces to a single sum by aligning the z -axis of the spherical coordinate system with the direction of the velocity

$$a_{\ell m}^{(\text{obs})} = \sum_{\ell'} K_{\ell m}^{\ell' m'}(\beta) a_{\ell' m}^{(\text{rest})} \quad , \quad (5)$$

which simplifies the computations drastically. This is due to the fact that in this special case the aberration causes angular distortions only in the direction of the polar angle ϑ . The aberration kernel in eq. (5) can be computed by the recursion algorithm of Chluba (2011), see also (Dai & Chluba 2014).

The multipole transformation leads to a coupling between nearby multipoles. Aligning the z -axis of the spherical coordinate system with the boost in the forward direction, the temperature fluctuation structures are compressed towards the north pole leading to a power leakage from C_ℓ to higher multipoles $C_{\ell+1}, C_{\ell+2}, \dots$ on the northern hemisphere. On the southern hemisphere, the power leakage occurs towards lower multipoles $C_{\ell-1}, C_{\ell-2}, \dots$ since the structures are stretched there. In full sky analyses these power redistributions partly cancel, and in partial sky analyses, special care has to be taken into account (Catena & Notari 2013). Methods to detect these mode couplings between neighbouring multipoles were suggested by Bures & Rappaport (2006); Kosowsky & Kahniashvili (2011) and Amendola et al. (2011). The Planck Collaboration: Aghanim et al. (2014) finds the mode couplings to be consistent with the peculiar velocity determined by the Doppler dipole. The dependence of the magnitude of the power leakage on the angular distance from the boost direction is analysed by Jeong et al. (2014) and discussed with respect to hemispherical asymmetries by Notari et al. (2014). These considerations are extended to the polarization measurements of the CMB in (Amendola et al. 2011; Dai & Chluba 2014; Mukherjee et al. 2014; Yasini & Pierpaoli 2017, 2020).

In real sky observations, one has always to deal with a masked sky which also leads to a power leakage in neighbouring multipoles (see e. g. Catena & Notari (2013)). Therefore, the so-called pseudo- C_ℓ 's possess a mode coupling due to the aberration effect and to the partial sky observations. So one might alternatively turn to quantities that can be derived from local CMB data without the necessity to extract pseudo- $a_{\ell m}$'s obtained from the harmonic analysis on the full sky. This can be done by considering quantities de-

rived from the first and second covariant derivatives on the sphere with respect to ϑ and φ . These derivatives, however, depend on the chosen z -axis of the spherical coordinate system. Using these derivatives directly would be a drawback analogously to some methods employing strength of the mode coupling with respect to the angular distance from the boost direction. It is much more favourable to construct from the covariant derivatives with respect to ϑ and φ scalar quantities which are independent of the chosen z -axis. Out of the many possibilities, Monteserín et al. (2005) suggest twelve such scalar quantities suitable for general applications to the cosmic microwave background. All of them are based on the first and second covariant derivatives of the temperature field $\delta T(\vartheta, \varphi)$. Doré et al. (2003) discuss the geometrical meaning of the local curvature structure in the form as 'hill', 'lake' and 'saddle' regions.

It is the aim of this work to investigate which scalar statistics on the sphere suggested by Monteserín et al. (2005) are useful as an alternative method for the determination of our peculiar velocity.

2 SCALAR MEASURES ON THE SPHERE

The first covariant derivatives of the temperature field $\delta T(\vartheta, \varphi)$ are the usual partial derivatives denoted by a comma. As usual, the covariant derivatives are denoted by semicolons. The second covariant derivatives

$$\delta T_{;ij} = \delta T_{,ij} - \Gamma_{ij}^k \delta T_{,k} \quad , \quad i, j, k \in \{\vartheta, \varphi\} \quad , \quad (6)$$

require the Christoffel symbols Γ_{ij}^k which are non-vanishing only for $(ds^2 = d\vartheta^2 + \sin^2 \vartheta d\varphi^2)$

$$\Gamma_{\varphi\vartheta}^\varphi = \Gamma_{\vartheta\varphi}^\varphi = \frac{\cos \vartheta}{\sin \vartheta} \quad \text{and} \quad \Gamma_{\varphi\varphi}^\vartheta = -\sin \vartheta \cos \vartheta \quad .$$

The twelve scalars suggested by Monteserín et al. (2005) can be classified into the following groups:

- (i) Scalars derived from the Hessian matrix

The negative Hessian matrix $-\mathcal{H} = (-\delta T_{;ij})$ has as interesting quantities the eigenvalues, the trace and the determinant. The eigenvalues λ_1 and λ_2 can be expressed by the covariant derivatives as

$$\lambda_1 = -\frac{1}{2} \delta T_{;i}^{;i} + \frac{1}{2} \sqrt{(\delta T_{;i}^{;i})^2 - 2(\delta T_{;i}^{;i} \delta T_{;j}^{;j} - \delta T_{;i}^{;j} \delta T_{;j}^{;i})} \quad (7)$$

and

$$\lambda_2 = -\frac{1}{2} \delta T_{;i}^{;i} - \frac{1}{2} \sqrt{(\delta T_{;i}^{;i})^2 - 2(\delta T_{;i}^{;i} \delta T_{;j}^{;j} - \delta T_{;i}^{;j} \delta T_{;j}^{;i})} \quad . \quad (8)$$

The trace of the Hessian matrix \mathcal{H} corresponds also to the Laplacian and can be expressed by the eigenvalues

$$\lambda_+ = \text{tr } \mathcal{H} = \delta T_{;i}^{;i} = -\lambda_1 - \lambda_2 \quad . \quad (9)$$

And finally, the determinant of the negative Hessian matrix is

$$d = -\det \mathcal{H} = \frac{1}{2} \left[\delta T_{;i}^{;i} \delta T_{;j}^{;j} - \delta T_{;i}^{;j} \delta T_{;j}^{;i} \right] = \lambda_1 \lambda_2 \quad . \quad (10)$$

- (ii) Distortion scalars

The four scalars, which are chosen to characterize the distortion of the temperature field $\delta T(\vartheta, \varphi)$, are the shear, the

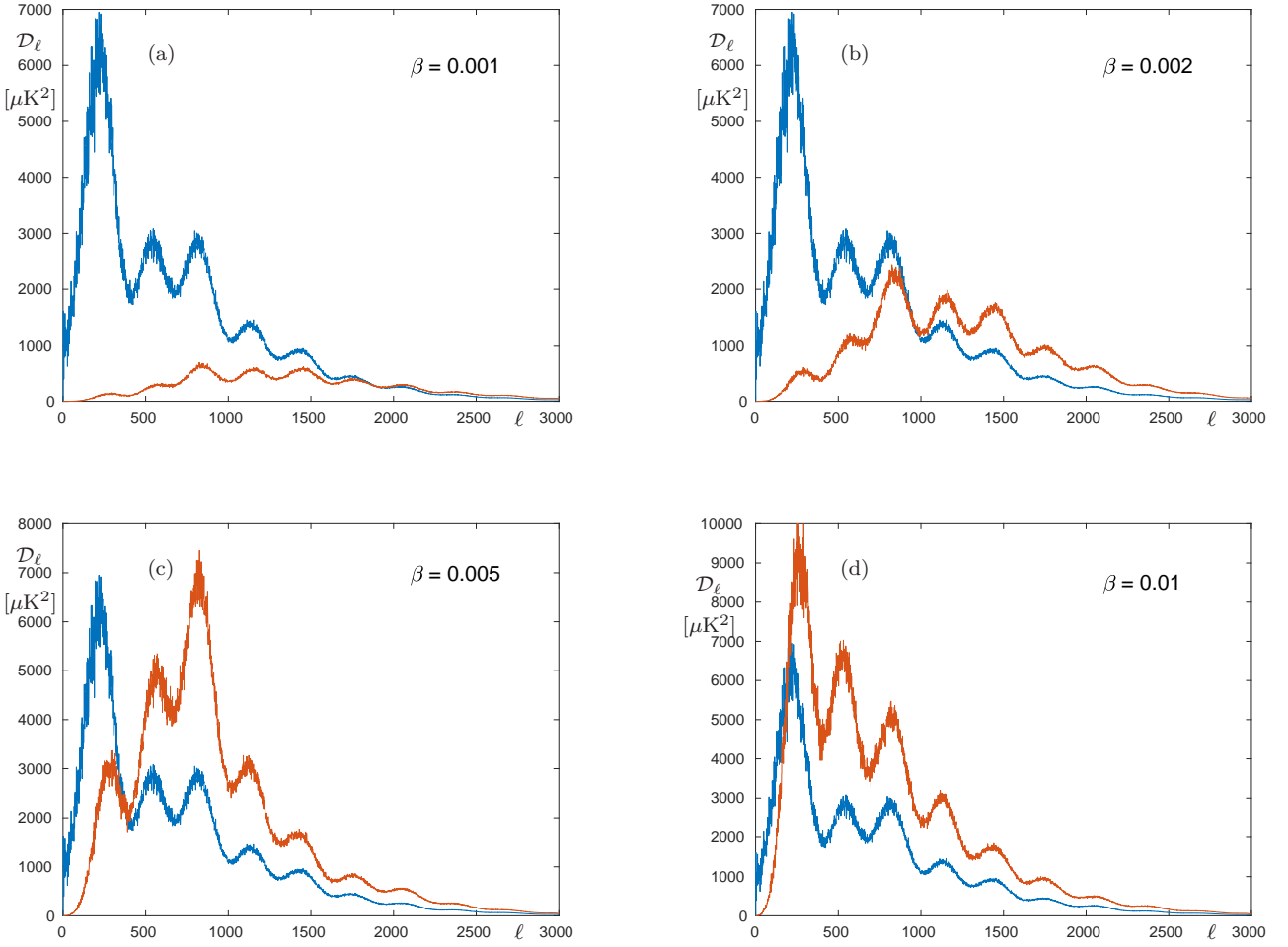


Figure 1. The multipole shifting spectra $\Delta\mathcal{D}_\ell = \ell(\ell + 1)\Delta C_\ell/(2\pi)$ with ΔC_ℓ defined in eq. (19) are plotted in red for four different peculiar velocities β . In addition, the corresponding CMB rest frame angular power spectrum $\mathcal{D}_\ell = \ell(\ell + 1)C_\ell^{(\text{rest})}/(2\pi)$ is shown as the same blue curve in all four panels in order to allow a comparison. All four cases are based on the same CMB rest frame realization.

distortion, the ellipticity and the shape index. They are defined as follow. The shear y is given as

$$\begin{aligned} y &= \frac{1}{4} [\delta T_{;i}^{;i}]^2 - \frac{1}{2} [\delta T_{;i}^{;i} \delta T_{;j}^{;j} - \delta T_{;i}^{;j} \delta T_{;j}^{;i}] \\ &= \frac{1}{4} (\lambda_1 - \lambda_2)^2, \end{aligned} \quad (11)$$

the distortion λ_- as

$$\lambda_- = \sqrt{[\delta T_{;i}^{;i}]^2 - 2 [\delta T_{;i}^{;i} \delta T_{;j}^{;j} - \delta T_{;i}^{;j} \delta T_{;j}^{;i}]} = \lambda_1 - \lambda_2, \quad (12)$$

the ellipticity e as

$$\begin{aligned} e &= -\frac{1}{2 [\delta T_{;i}^{;i}]} \sqrt{[\delta T_{;i}^{;i}]^2 - 2 [\delta T_{;i}^{;i} \delta T_{;j}^{;j} - \delta T_{;i}^{;j} \delta T_{;j}^{;i}]} \\ &= \frac{1}{2} \frac{\lambda_1 - \lambda_2}{\lambda_1 + \lambda_2}, \end{aligned} \quad (13)$$

and the shape index ι as

$$\iota = \frac{2}{\pi} \arctan\left(-\frac{1}{2e}\right). \quad (14)$$

(iii) Scalars derived from the gradient

The squared modulus of the gradient field and its derivative are considered here to extract the level of smoothness of the temperature field. The square of the gradient modulus g is given as

$$g = \delta T^{;i} \delta T_{;i}, \quad (15)$$

and a derivative of it as

$$D_g = \frac{d}{ds} \left(\frac{1}{2} g \right) = \delta T^{;ij} \delta T_{;i} \delta T_{;j}, \quad (16)$$

where the derivative has to be taken along the arc s associated to the integral curve of the gradient.

(iv) Curvature scalars

The last two scalars considered here are the Gaussian curvature

$$\kappa_G = \frac{1}{2} \frac{\delta T_{;i}^{;i} \delta T_{;j}^{;j} - \delta T_{;i}^{;j} \delta T_{;j}^{;i}}{(1 + [\delta T^{;i} \delta T_{;i}])^2} \quad (17)$$

and the extrinsic curvature being the average of the two principal curvatures of the temperature field can be expressed by

the quantities defined so far

$$\kappa_{\text{ex}} = \frac{1}{2} \frac{1}{\sqrt{1+g}} \left[\lambda_+ - \frac{D_g}{1+g} \right]. \quad (18)$$

For further details on these twelve scalar measures, see the discussions in [Monteserín et al. \(2005\)](#).

3 THE ABILITY OF SCALAR MEASURES TO DETECT THE ABERRATION

All the scalar measures presented in the previous section are based on covariant derivatives on the temperature field $\delta T(\vartheta, \varphi)$ and are independent of the chosen orientation of the spherical coordinate system. But they differ in the ability to detect the distortions caused by the aberration. In order to find the most suitable scalar measures, these measures are computed from a set of 1000 simulated CMB sky maps such that the deviation of the detected boost direction from that used in the simulations allows such a decision.

The CMB simulations are based on the power spectrum which is computed using CAMB¹ for the cosmological parameters of the Λ CDM concordance model given by the [Planck Collaboration: Aghanim et al. \(2020\)](#) in their table 6 in the column ‘Planck+BAO’. The main parameters are $\Omega_b h^2 = 0.022447$, $\Omega_c h^2 = 0.11923$, and $h = 0.677$. A large set of CMB sky map realizations is generated from this power spectrum which yields the spherical expansion coefficients $a_{\ell m}^{(\text{rest})}$ in the CMB rest frame. Then these sky maps are boosted in the z -direction using eq. (5) for several peculiar velocities β in order to obtain the coefficients $a_{\ell m}^{(\text{obs})}$. The aberration kernel is computed by the recursion algorithm of [Chluba \(2011\)](#). To allow a decision on the quality of the scalar measures of section 2 free of numerical artefacts, all computations are carried out in harmonic space up to the multipole order of $\ell_{\text{max}} = 3000$, so that the required differentiations with respect to ϑ and φ are also computed from the coefficients $a_{\ell m}^{(\text{obs})}$. Only in the final step, the sky maps of the scalar measures are generated in the HEALPix format ([Górski et al. 2005](#)) with a resolution of $N_{\text{side}} = 2048$.

The effect of the aberration can be studied in the multipole spectra C_ℓ by considering the relative difference $(C_\ell^{(\text{obs})} - C_\ell^{(\text{rest})})/C_\ell^{(\text{rest})}$ as done by [Jeong et al. \(2014\)](#) which is considering boosted values $C_\ell^{(\text{obs})}$ minus the rest frame values $C_\ell^{(\text{rest})}$ in the power spectrum. Another instructive possibility is to consider the difference in the expansion coefficients $a_{\ell m}$ by defining the multipole shifting spectra

$$\Delta C_\ell = \frac{1}{2\ell+1} \sum_{m=-\ell}^{\ell} |a_{\ell m}^{(\text{obs})} - a_{\ell m}^{(\text{rest})}|^2. \quad (19)$$

The effect of boosting the CMB radiation by four different velocities β is shown in figure 1 where the multipole shifting power spectrum $\Delta \mathcal{D}_\ell = \ell(\ell+1)\Delta C_\ell/(2\pi)$ with ΔC_ℓ defined above in eq. (19) is plotted in comparison with the CMB rest frame angular power spectrum $\mathcal{D}_\ell = \ell(\ell+1)C_\ell^{(\text{rest})}/(2\pi)$. The peculiar velocity $\beta = 0.001$, which is shown in figure 1(a), is close to our solar system value $\beta_\odot = 0.00123$ and reveals

¹ The software was written by A. Lewis and A. Challinor and may be downloaded from <http://camb.info/>

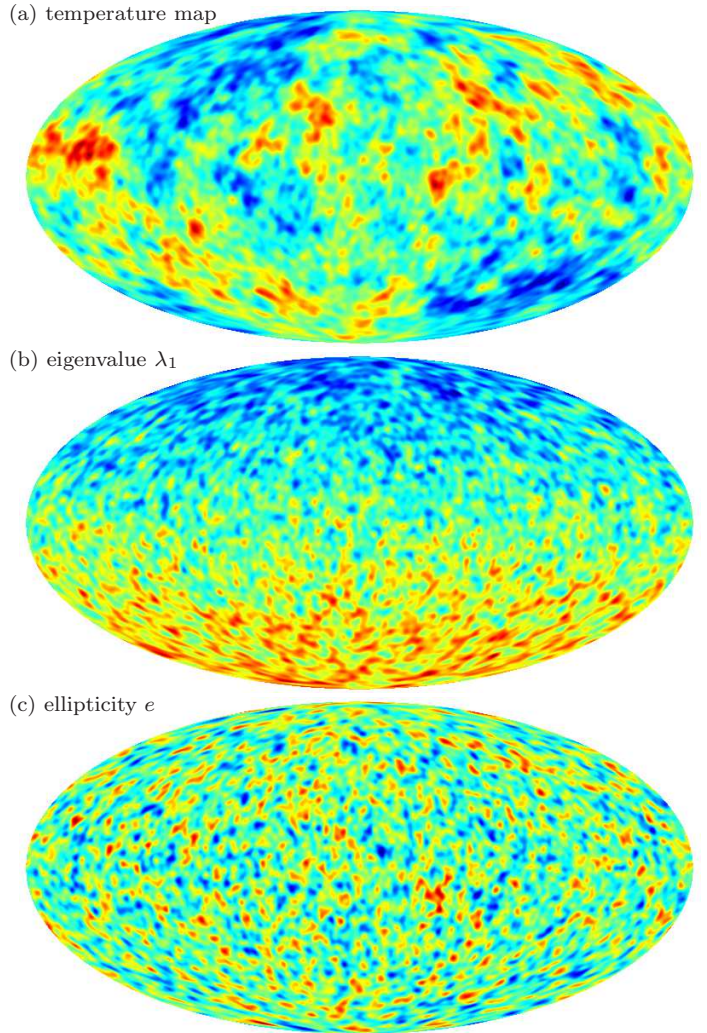


Figure 2. The aberrated temperature map is shown in panel (a), where a peculiar velocity of $\beta = 0.01$ in the z -direction is used. The motion is thus towards the north pole (“above”) in this Mollweide projection. The panel (b) presents the eigenvalue λ_1 defined in eq.(7). Finally, panel (c) displays the ellipticity e given in eq.(13). In order to enhance the visibility of the aberration effect, all three maps are smoothed in a final step by a Gaussian with a FWHM of 3° .

an appreciable influence of the aberration above $\ell \gtrsim 800$. At multipoles above $\ell \simeq 2000$ the multipole shifting power spectrum $\Delta \mathcal{D}_\ell$ becomes even larger than \mathcal{D}_ℓ in this case. For increasingly larger values of β , the multipole shifting power spectrum $\Delta \mathcal{D}_\ell$ begins to dominate at ever smaller multipole orders as seen in figures 1(b) to 1(d). However, for the most interesting case of the solar system barycentre velocity, one has to carry out the analysis with sufficiently high multipole orders and thus, all calculations of this work are done with a cut-off of $\ell_{\text{max}} = 3000$.

In order to demonstrate that the twelve scalar measures presented in section 2 are not all suited on the same footing to extract the modifications due to the aberration, two examples of them are given in figure 2, where the velocity $\beta = 0.01$ is used. The panel 2(a) shows the aberrated temperature map obtained from the CMB rest frame by applying the velocity $\beta = 0.01$ in the z -direction which corresponds

to the north pole (“above”) in these sky maps. The aberration effect is almost invisible. This changes drastically by computing the sky map which shows the value of the first eigenvalue λ_1 of the Hessian matrix instead of the aberrated temperature as revealed by panel 2(b). One recognizes a significant dipole contribution although the CMB rest frame realization has none, since its quadrupole contribution is the first non-vanishing multipole. As an example from the group of distortion measures, the figure 2(c) displays the ellipticity e defined in eq.(13), and there is no asymmetry between the Northern and the Southern hemisphere, which could reveal a non-vanishing peculiar velocity. It should be noted that in all three panels of figure 2, a Gaussian smoothing with a full width half-maximum (FWHM) of 3° is applied after the scalar measures are calculated from the expansion coefficients $a_{\ell m}^{(\text{obs})}$ of the unsmoothed temperature map with $\ell_{\text{max}} = 3000$.

Since figure 2 has emphasized that the scalar measures of section 2 are very different in their discriminating power to extract the aberration effects, it is therefore natural to ask for the best-suited quantity. To that aim a set of 1000 CMB realizations is generated using the peculiar velocity $\beta_\odot = 0.00123$ and $\ell_{\text{max}} = 3000$. The boost is chosen in the z -direction and the twelve scalar measures are computed from these 1000 aberrated CMB simulations. In the next step, the dipole of each of the 1000 maps for each of the twelve scalar measures is extracted which allows the determination of the orientation of the dipole. The agreement or the deviation of this orientation from the boost orientation chosen in the simulations reveals the usability of the considered scalar measure. In spherical coordinates, the direction of the z -axis is given by the polar angle $\vartheta = 0$ which thus defines the correct forward direction. The backward direction corresponds then to $\vartheta = \pi$, of course. A suitable scalar measure should thus yield a value close to $\vartheta = 0$ for the forward direction and close to $\vartheta = \pi$ for the backward direction. The distributions of the orientations obtained in this way are shown in the histograms in figure 3. The bin width of histograms should be equal for the variable $x = \cos \vartheta$, so that each bin refers to the same size of the corresponding solid angle. Thus, the histograms discussed in the following cover the interval from $\cos \vartheta = -1$ to $\cos \vartheta = 1$.

The normalized histograms in figure 3 show the probability distribution of $\cos \vartheta$ where the polar angle ϑ is determined from the orientation of the dipole $\ell = 1$ of the corresponding twelve scalar measures. In order to compute this dipole orientation, all expansion coefficients $a_{\ell m}$ are set to zero except those three belonging to $\ell = 1$ from which a sky map is generated whose maximal and minimal values yield the dipole orientation. Each panel in figure 3 displays two histograms, one reveals the angle ϑ obtained from the maximum of the dipole and the other from the minimum. As might be expected from figure 2, the eigenvalue λ_1 has a good discriminating power as revealed by the sharp peaks in the histogram at $\cos \vartheta = -1$ and $\cos \vartheta = 1$. The same applies to the other eigenvalue λ_2 although the orientation of the dipole is swapped. The panel 3(c) presents the histogram of the Laplacian λ_+ given in eq. (9). Although the aberration direction is recognized in a lot of realizations, there are also many false detections as revealed by the non-vanishing bins even close to the equator. This distracting feature is absent for the determinant d of the Hessian matrix, although the comparison of its histogram with those of the eigenvalues λ_1

and λ_2 uncovers a greater width and thus, a more unreliable detection of the boost direction. The histograms in figures 3(e) to 3(h) corresponds to the group of distortion measures. The histograms reveal a good discriminating power for the shear y and for the distortion λ_- , while the ellipticity e and the shape index ι are unusable as seen by the equidistributed histograms. The sky map corresponding to the ellipticity e was already shown in figure 2(c), where also no boost signature was noticeable. The square of the gradient modulus g is able to detect the boost direction as seen in figure 3(i), but it is more unreliable than the eigenvalues λ_1 or λ_2 as one observes from the width of the histograms. The derivative D_g peaks also towards the peculiar velocity, but it is indifferent with respect to its direction as seen in figure 3(j). Finally, the last two panels reveal that the Gaussian curvature κ_G as well as the extrinsic curvature κ_{ex} are unsuitable due to the equidistributed histograms.

Since there are four scalar measures with a good detection characteristic as follows from the discussion of figure 3, it is more quantitative to consider the median of their distributions. The median values of the angular difference of direction of the dipole from the boost direction is listed in table 1. In the anti-boost direction, the listed value should be compared with $\vartheta = 180^\circ$. One observes from table 1 that the best scalar measures are the two eigenvalues λ_1 and λ_2 , the shear y and the distortion λ_- . Although the square of the gradient modulus g is more easily computed, since only first order derivatives are needed, its median is roughly twice as large as for the four best measures. These median values are computed by using the solar system velocity and, of course, would yield more accurate results for higher velocities.

The eigenvalues λ_1 and λ_2 determine not only the direction of the peculiar velocity but also its modulus. This is demonstrated in figure 4 where the maximal value $D_{\lambda_1}(\beta)$ of the dipole of λ_1 is plotted for several different values of the peculiar velocity β . One observes a linear behaviour such that the amplitude of the dipole can be used to estimate also the magnitude of the velocity. The linear behaviour is well approximated by the fit

$$D_{\lambda_1}(\beta) = c_1 \beta + c_0 \quad (20)$$

with

$$c_1 = (79.10 \pm 0.48) \times 10^6 \mu\text{K} \quad (21)$$

and

$$c_0 = -(783 \pm 2656) \mu\text{K} \quad , \quad (22)$$

where the coefficients are determined from the simulations based on the Λ CDM model specified above. The inset in figure 4 displays the distribution of the maximal values $D(\beta)$ for the 1000 simulations for the case $\beta_\odot = 0.00123$ which possess a standard deviation of $\sigma = 12699 \mu\text{K}$ around the mean value $D_{\lambda_1}(\beta_\odot) = 94391 \mu\text{K}$. The standard deviation σ is of the same order for the other considered values of β . Since the fit value for c_0 is compatible with zero, the constant c_0 can be neglected. Thus, if the observations would determine D_{λ_1} with sufficient accuracy, the modulus of velocity β could be determined with an accuracy of the order $\sigma/c_1 \simeq 1.6 \times 10^{-4}$.

Up to now, the peculiar velocity is solely determined from the dipole orientation extracted from the corresponding scalar measure. Thus, one might wonder whether the inclusion of higher multipoles could increase the accuracy. To that

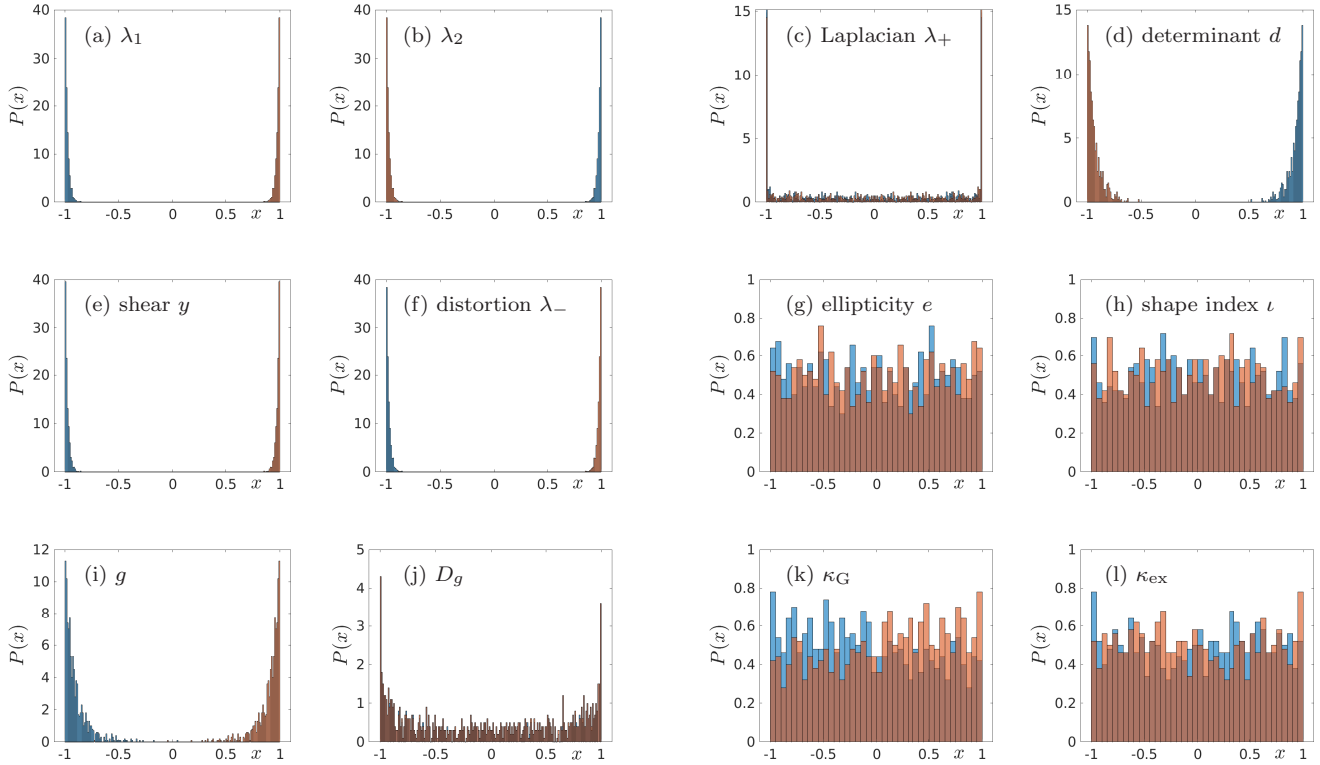


Figure 3. The probability distributions of the dipole orientations are shown obtained from 1000 CMB realizations for our solar system barycentre velocity $\beta_{\odot} = 0.00123$. The bins have an equal width with respect to $x = \cos \vartheta$ such that each bin corresponds to the same solid angle. The blue bins corresponds to the maximum of the dipole and the red ones to its minimum. The first row presents the distributions of the scalar measures derived from the Hessian matrix, while the second row displays the distortion scalars. The last row shows the square of the gradient modulus and its derivative as well as the two curvature measures. Four scalar measures possess an equidistribution. In these four cases, shown in panels (g), (h), (k), and (l), a larger bin width is chosen in order to suppress fluctuations.

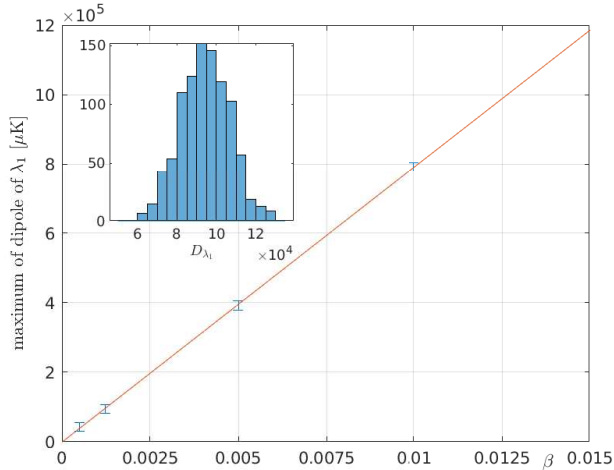


Figure 4. The maximum $D_{\lambda_1}(\beta)$ of the dipole of λ_1 is plotted as a function of the peculiar velocity β . The error bars show the 1σ deviation from the mean obtained from 1000 simulations for the values $\beta = 0.0005, 0.00123, 0.005$ and 0.01 . The linear fit given in eq. (20) is shown as a straight line. The inset displays the distribution of D_{λ_1} in units of μK of the 1000 realizations obtained for $\beta = \beta_{\odot}$.

Table 1. The median values of the polar angle ϑ of the distributions of the suitable scalar measures are listed, such that in 50% of the cases, a more accurate estimate of the velocity would be obtained. The median values are derived from 1000 aberrated CMB realizations with $\beta_{\odot} = 0.00123$. Since some scalar measures have their minimum of the dipole in the forward direction instead of the backward direction, the median direction of the minimum is additionally listed for convenience, which is related by $\vartheta_{\min} = 180^\circ - \vartheta_{\max}$.

Scalar measure	Median of dipole maximum	Median of dipole minimum
λ_1	170.5324°	9.4676°
λ_2	9.4676°	170.5324°
λ_+	91.4549°	88.5451°
d	17.416°	162.584°
y	170.498°	9.502°
λ_-	170.5324°	9.4676°
g	159.6431°	20.3569°

aim, the extrema in the sky maps computed from the sum of the dipole and the quadrupole contribution are also investigated. Because one might also worry about the sharp cut-off at $\ell = 2$ or $\ell = 3$, respectively, a strong smoothing with Gaussian of FWHM of 45° and of 90° is additionally taken into account. The results are presented in figure 5 for the example of the first eigenvalue λ_1 . The position of the minimum of the

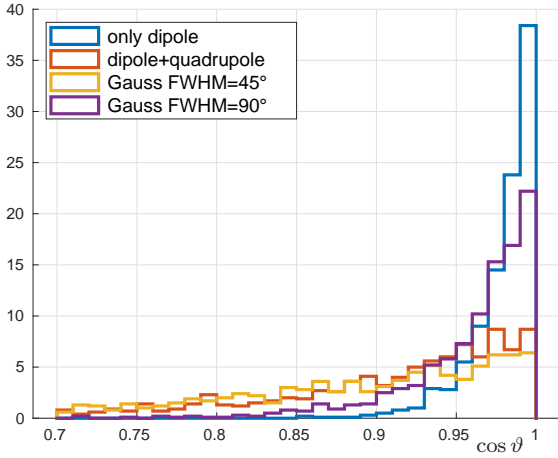


Figure 5. The distribution of the deviation $\cos\vartheta$ is determined from the sky map of the first eigenvalue λ_1 . The deviation angle ϑ is determined in three ways: (i) the orientation of the dipole by its minimum on the sphere, (ii) the minimum of the sum of the dipole and the quadrupole, and (iii) the minimum of the sky map obtained from a Gaussian smoothing with a FWHM=45° and with a FWHM=90° but retaining all multipoles.

values of λ_1 on the sphere are determined, which should point approximately in the boost direction $\vartheta = 0$. It is clearly seen that the sharpest distribution towards $\cos\vartheta = 1$ is obtained by using only the dipole. Taking higher multipoles into account leads to a smearing of the distribution and thus to a more unreliable estimate for the boost direction.

In the case of partial sky observations, one has to deal with the difficulty to determine the dipole in the presence of a masked sky. The dipole then has to be fitted to the map of the eigenvalue λ_1 in the observed part of the sky. The full sky analysis of this work leads to the suggestion that the best estimate for our peculiar velocity will probably be achieved by fitting the dipole to the unsmoothed map. Without smoothing one does not need to care about smoothing a masked sky which is usually carried out in the $a_{\ell m}$ space by multiplying the expansion coefficients $a_{\ell m}$ with $F_\ell = \exp(-\frac{1}{2}\alpha^2\theta_G^2\ell(\ell+1))$ and $\alpha = \pi/(180\sqrt{8\ln 2})$ if the smoothing θ_G is given in degrees. This requires the determination of the coefficients $a_{\ell m}$ from a partial sky observation with a probably complicated mask structure. We thus suggest a three parameter fit, which is the dipole amplitude and the two angles for its orientation, to the unsmoothed map using a least-squares fitting, for example. This can be achieved by minimizing the expression

$$S(\beta, \vartheta, \varphi) = \sum_i \frac{(p_{\text{dip}}^i(\beta, \vartheta, \varphi) - p^i)^2}{\sigma_i^2}, \quad (23)$$

where $p_{\text{dip}}^i(\beta, \vartheta, \varphi)$ denotes the dipole value at pixel i with the dipole orientation given by ϑ and φ . Furthermore, p^i is the value of the λ_1 map at pixel i and σ_i the estimated error for this pixel. The sum runs only over the observed pixels. This procedure should also be favourable to reduce the uncorrelated pixel-to-pixel noise. It is clear that observations of too small a fraction of the sky will not allow a reliable determination of the peculiar velocity.

4 CONCLUSION

The motion of our solar system relative to the CMB rest frame leads to the large CMB dipole and to subtle distortions in the CMB sky map due to the aberration effect. Our peculiar velocity is usually derived from the dipole component of the CMB sky. It is then assumed that the CMB dipole is a pure Doppler dipole and a further intrinsic dipole and secondary effects can be safely ignored. It is thus desirable to have an independent method for the determination of the peculiar velocity. The aberration effect leads to mode couplings in the angular power spectrum which can betray the motion as discussed in the Introduction. However, if one tries to circumvent the determination of the spherical harmonic expansion coefficients $a_{\ell m}$, one can consider covariant derivatives on the sphere which measure the extent of the distortions being a compression of structures in the forward direction and a stretching in the backward direction. This method thus requires CMB maps with sufficiently high resolution. But since no full sky expansion is required as long as the process of derivation can be carried out with the observational data, high-resolution partial data would be suitable as provided by the Simons Observatory (Ade et al. 2019) and by CMB-S4 (Abazajian et al. 2019). The direct use of the partial derivatives on the sphere with respect to the coordinates ϑ and φ has the disadvantage that they depend on the orientation of the spherical coordinate system. This is circumvented by the use of scalar measures, where in this work the twelve scalar quantities suggested by Monteserín et al. (2005) are investigated. The main result is that the eigenvalues λ_1 and λ_2 of the Hessian matrix defined in eqs.(7) and (8), the shear y and the distortion λ_- given in (11) and (12), respectively, are the best choices for detecting the boost direction. The remaining eight scalar quantities are not well-suited for this task. And it is demonstrated that the peculiar velocity is most accurately determined by extracting only the dipole contribution from the four favourable scalar measures.

ACKNOWLEDGEMENTS

The software packages HEALPix (<http://healpix.jpl.nasa.gov>, Górski et al. (2005)) and CAMB written by A. Lewis and A. Challinor (<http://camb.info/>) as well as the Planck data from the LAMBDA website (<http://lambda.gsfc.nasa.gov>) were used in this work. Furthermore, we would like to thank the unknown referee for his useful comments.

DATA AVAILABILITY

The data underlying this article will be shared on reasonable request to the corresponding author.

REFERENCES

- Abazajian K., et al., 2019, arXiv:1907.04473
 Ade P., et al., 2019, *J. Cosmology Astropart. Phys.*, 2019, 056
 Amendola L., Catena R., Masina I., Notari A., Quartin M., Quercellini C., 2011, *J. Cosmology Astropart. Phys.*, 07, 027
 Burles S., Rappaport S., 2006, *ApJ*, 641, L1

- Catena R., Notari A., 2013, *J. Cosmology Astropart. Phys.*, 04, 028
- Challinor A., van Leeuwen F., 2002, *Phys. Rev. D*, 65, 103001
- Chluba J., 2011, *MNRAS*, 415, 3227
- Dai L., Chluba J., 2014, *Phys. Rev. D*, 89, 123504
- Doré O., Colombi S., Bouchet F. R., 2003, *MNRAS*, 344, 905
- Górski K. M., Hivon E., Banday A. J., Wandelt B. D., Hansen F. K., Reinecke M., Bartelmann M., 2005, *ApJ*, 622, 759
- Jeong D., Chluba J., Dai L., Kamionkowski M., Wang X., 2014, *Phys. Rev. D*, 89, 023003
- Kim J., Naselsky P., 2010, *ApJ*, 714, L265
- Kogut A., et al., 1993, *ApJ*, 419, 1
- Kosowsky A., Kahnishvili T., 2011, *Phys. Rev. Lett.*, 106, 191301
- Land K., Magueijo J., 2005, *Phys. Rev. D*, 72, 101302
- Monteserín C., Barreiro R. B., Sanz J. L., Martínez-González E., 2005, *MNRAS*, 360, 9
- Mukherjee S., De A., Souradeep T., 2014, *Phys. Rev. D*, 89, 083005
- Notari A., Quartin M., Catena R., 2014, *J. Cosmology Astropart. Phys.*, 03, 019
- Planck Collaboration: Aghanim N., et al., 2014, *A&A*, 571, A27
- Planck Collaboration: Aghanim N., et al., 2020, *A&A*, 641, A1
- Planck Collaboration: Akrami Y., et al., 2020, *A&A*, 641, A7
- Yasini S., Pierpaoli E., 2017, *Phys. Rev. D*, 96, 103502
- Yasini S., Pierpaoli E., 2020, *MNRAS*, 493, 1708